Effect of angular momentum on giant dipole resonance observables in the $^{28}Si + ^{116}Cd$ reaction

Ish Mukul,* A. Roy, P. Sugathan, J. Gehlot, G. Mohanto, N. Madhavan, S. Nath, and R. Dubey
Inter University Accelerator Centre, Aruna Asaf Ali Marg, New Delhi 110067, India

I. Mazumdar and D. A. Gothe
Department of Nuclear and Atomic Physics, Tata Institute of Fundamental Research, Homi Bhabha Road, Mumbai 400005, India

Maninder Kaur
Department of Physics, Panjab University, Chandigarh 160014, India

A. K. Rhine Kumar and P. Arumugam
Department of Physics, Indian Institute of Technology Roorkee, Roorkee 247667, Uttarakhand, India

(Received 1 July 2013; published 16 August 2013)

Background: Giant dipole resonance (GDR) has been used as an important tool for studying nuclear properties in hot rotating nuclei. Exclusive measurements using low-energy γ-ray multiplicity filters provide more control over angular momentum selection in such measurements.
Purpose: Study the effect of angular momentum and temperature on nuclear deformations and GDR widths at high excitation energies in ^{144}Sm.
Methods: Exclusive measurements of GDR γ rays were carried out in the $^{28}Si + ^{116}Cd$ reaction populated at two different excitation energies. Beam energies of 125 and 140 MeV pumped the nuclei to average temperatures $\langle T \rangle$ of 1.1 to 1.5 MeV. The high-energy γ rays were measured using the large NaI(Tl) detector in coincidence with the sum-spin multiplicity filter consisting of 32 NaI(Tl) detectors covering nearly 4π sr of solid angle.
Results: The average angular momentum $\langle J \rangle$ spanned the range of $25\hbar$ to $60\hbar$. The GDR centroid energies, widths, and deformation parameter (β) were extracted as a function of $\langle J \rangle$ at three different $\langle T \rangle$ bins of 1.1, 1.3, and 1.5 MeV. The thermal shape fluctuation model (TSFM) calculations have been performed incorporating the fluctuations induced due to temperature and deformation in the nucleus using a numerically exact method. The calculations showed evidence of deformation throughout the experimental range. The GDR width data have been interpreted in terms of reduced width as a function of reduced angular momentum.
Conclusions: The nucleus evolves to a deformed shape from spherical shape in ground state in the extracted temperature range as predicted by the theoretical calculations. Kusnezov's parametrization also holds good for the large experimental J range.

DOI: 10.1103/PhysRevC.88.024312 PACS number(s): 24.30.Cz, 25.70.Jj, 24.60.Dr, 27.60.+j

I. INTRODUCTION

Collective modes of excitations in many-body systems have been an active field of research for a long time. In atomic nuclei, these modes of excitations provide a better tool for study of nuclear shapes and deformations at high excitation energies. Out of several modes of excitation, giant dipole resonance (GDR) provides close insight into the nuclear shapes of hot rotating nuclei at high excitation energies [1,2]. Heavy-ion fusion reactions populate compound nuclei (CN) over a wide range of angular momenta (J) and excitation energies (E^*) which in turn give rise to increase in the temperature (T) of the system. The excited CN may undergo fission or decays with the emission of neutrons, charged particles, and GDR γ rays. The GDR centroid energy is inversely proportional to the nuclear radius, providing direct information on the deformation in the excited nucleus, and the GDR width provides a measure of the damping mechanism of the resonance. Studying these GDR properties as a function of J and T provides a better understanding of the behavior of a nucleus at excited states. A major experimental challenge in the study of shape evolution using GDR measurement is the entangling of the effects of J and T in the measured high-energy γ-ray spectra. At a given excitation energy, the increase in J reduces the effective T of the system. Hence to study the evolution of nuclear shapes, it is important to decouple the spin effects by selecting a narrow J window on the experimental spectrum. The J dependence of GDR can be determined by measuring the high-energy γ-ray spectra in coincidence with low-energy yrast γ-ray multiplicity. These low-energy γ rays are isotropic and a high-efficiency detector system can provide more control over J selection in such measurements. With the availability of modern large γ-ray multiplicity detector arrays, it has become possible to measure the effect of J on GDR γ rays and study of shape evolution at high excitation energies.

The effects of angular momentum on GDR built on excited states have been studied by several groups over a wide mass region using heavy-ion-induced fusion reactions. These studies have provided systematic information on the variation of GDR observables for $T < 2$ MeV. In the past few decades, exclusive GDR measurements in medium-heavy mass region

*ishmukul@gmail.com

using γ-ray multiplicity filters have been done in ^{86}Mo [3], ^{113}Sb [4], ^{147}Eu [5], ^{152}Gd [6],^{162}Yb [7], and ^{176}W [8]. According to these results, it is shown that the GDR width increased with T whereas J seems to affect it only for $J > 30\hbar$. The centroid energy remains the same for individual masses over wider ranges of J and T. Theoretically different models such as the collisional damping model [9,10], the phonon damping model [11,12], and the thermal shape fluctuation model (TSFM) [13–17] have been proposed to explain the evolution of GDR properties as a function of J and T. Of these, TSFM in general has been reasonably successful in explaining most of the experimental data for $T < 2$ MeV. Based on TSFM, Kusnezov *et al.* [18] proposed a phenomenological function to scale GDR widths as a function of J, T, and A. Although the results from different mass regions provide some insight to the GDR systematics in general, it is still necessary to perform experiments for each mass region to study the evolution of intrinsic GDR properties with J and T.

In this paper, we report the GDR measurement on ^{144}Sm and its J dependence over different T regions. The nucleus ^{144}Sm has a spherical shape in the ground state with its resonance centroid at 15.3 MeV and a width of 4.37 MeV [19]. From theoretical predictions, it has been shown that this nucleus may exhibit different shapes in the T range of 1.1 to 1.5 MeV. It is therefore interesting to study GDR width evolution and deformations for this nuclei from the ground state to some finite temperature. In the present experiment, we extracted the GDR parameters for ^{144}Sm as a function of J at different T using the reaction $^{28}\mathrm{Si} + {}^{116}\mathrm{Cd}$, at two different beam energies. To explain the results, we have applied the TSFM incorporating the shape fluctuations in this system.

II. EXPERIMENTAL DETAILS

The experiment was performed using the Pelletron facility at the Inter-University Accelerator Centre (IUAC), New Delhi. Isotopically enriched ^{116}Cd target (more than 98% enrichment) was bombarded by a ^{28}Si beam at two laboratory energies forming the CN ^{144}Sm at different excitation energies. Self-supporting targets of thickness $\sim$1.8 mg/cm^2 and 2.0 mg/cm^2 were prepared at the IUAC target laboratory by rolling ^{116}Cd foils. The beam energy was chosen to be 125 and 140 Mev to excite the CN at 68 and 80 MeV respectively (after correcting the energy loss through half the thickness of the target). The relevant parameters calculated for the reactions are tabulated in Table I.

The high energy γ rays were detected using the high energy gamma ray spectrometer (HiGRaSp) [21] at IUAC. The spectrometer consists of a large cylindrical NaI(Tl) crystal measuring 25.4 cm $\times$ 30.5 cm. Four plastic scintillator detectors surrounded the NaI(Tl) as active shields for rejection of cosmic muons. The detector system was positioned at a distance of 80 cm from the target center at an angle of 90° with respect to the beam direction. To eliminate the chance of the beam hitting the target frame, a tantalum collimator with a slit size of 4 mm $\times$ 4 mm was placed in the beam line at a distance of $\sim$50 cm upstream from the target position. The γ-rays and neutrons originating from the collimator were shielded by lead and borated polythene bricks for stopping γ rays and neutrons, respectively. Standard Nuclear Instrumentation Module (NIM) electronics was used to process the energy and timing signals from the detector. The dynode signals after gain matching were fed to spectroscopic amplifiers and summed to get the total energy information. Fast timing from the anode was used to start various time-to-amplitude converter (TAC) modules. In order to eliminate piled up events, a pileup (PU) detection circuit [22] was implemented using the zero-cross timing of the bipolar signal from the HiGRaSp dynode. Energy calibration for HiGRaSp was performed using 662, 1173, and 1332 keV γ rays from ^{137}Cs and ^{60}Co sources. The sum peak of 2.505 MeV from ^{60}Co and the 4.438 MeV γ line from an Am-Be neutron source yielded other calibration points. Energy gain was monitored offline every 6 hours using these sources and in-beam monitoring was performed using the neutron capture peak at 6.83 MeV. Energy gain was found to be stable throughout the experimental duration. The response of the detector for different monoenergetic γ rays was generated using the Monte Carlo simulation package GEANT4 [23].

TABLE I. Fusion cross section (σ_f), excitation energy (E^*), and angular momentum (J_0) values calculated using CASCADE [20].

E_{beam} (MeV)	σ_f (mb)	E^* (MeV)	J_0 ($\hbar$)
125	925	68	38
140	550	80	54

The 32-element 4π sum-spin spectrometer [24] was used to measure the total multiplicity of low-energy γ rays. The multiplicity filter consists of 32 closely packed NaI(Tl) detectors in soccer-ball geometry (20 hexagonal and 12 pentagonal faces) covering a solid angle of $\sim 4\pi$ sr. In the present experiment only 27 detectors were used with a solid angle coverage of 82% of 4π sr. The target was positioned at the geometrical center of the 4π array. The detection threshold for each detector was kept at $\sim$100 keV. The total γ-ray multiplicity and time information were recorded online. A clear separation of γ rays and neutrons was achieved by recording time of flight (TOF) between the HiGRaSp and multiplicity filter. An anticoincidence plastic shield ensured the reduction of the cosmic ray background. A Computer Automated Measurement and Control (CAMAC) based multiparameter data acquisition software CANDLE [25] was used to record online events based on the trigger condition satisfying the logical AND of the TOF, PU condition, and energy threshold of $\sim$4 MeV. The list mode parameters consisted of energy, TOF, γ-fold, and PU events.

III. EXPERIMENTAL DATA ANALYSIS

Offline data analysis was performed in two parts: (a) extraction of high-energy γ-ray spectra from experimental data and (b) the comparison of extracted spectra with statistical model calculations to extract GDR parameters. These are described in details below.

A. Experimental data reduction

Using the CANDLE software, one-dimensional histograms were generated on an event-by-event basis for various

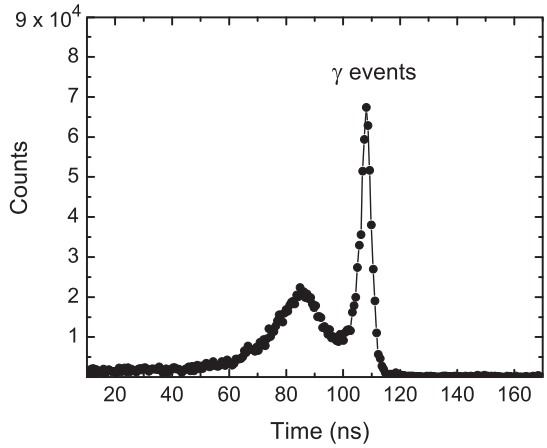

FIG. 1. A time of flight (TOF) spectrum showing clear separation of neutron and γ-ray events for 140 MeV beam energy. The spectrum is gated with the condition of fold 6 and above.

parameters such as γ-ray energy, TOF, and γ-fold distribution. A typical TOF spectrum showing clear separation between neutron and gamma events is shown in Fig. 1. The prompt γ-ray peak in the TOF spectrum was used to gate the high-energy γ-ray spectrum thereby selecting only the γ-ray events in the large NaI(Tl) detector. Further cleaning of the spectra has been done by eliminating pileup events. The signals from plastic scintillators were separately used as vetoes in the offline analysis to eliminate any residual random cosmic events. Fold-gated spectra were obtained by gating these cleaned spectra with respective folds. Similar fold-gated high-energy γ-ray spectra were generated by taking a random gate in the TOF spectrum, of similar width. These spectra were subtracted from the main γ-ray spectra to get rid of random in-beam

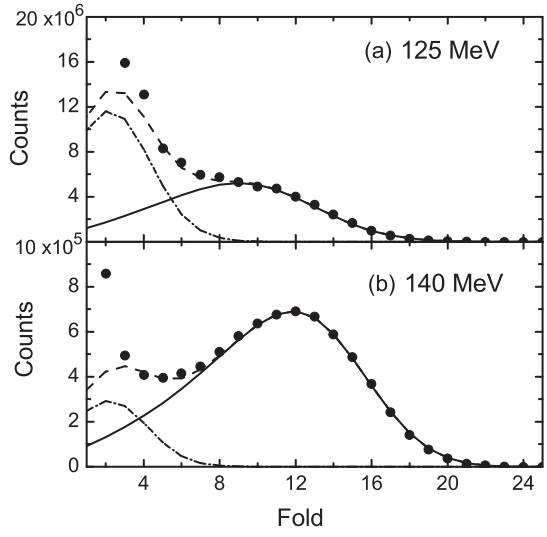

FIG. 2. Experimental and simulated fold distributions at beam energies of (a) 125 MeV and (b) 140 MeV. Simulated fold distributions generated using *P(M)* distribution [see Eq. (2)] and experimental points are depicted by solid lines and circles, respectively. A low multiplicity component is shown by the short-dash–dotted line and the total simulated distribution is given by the dashed line.

TABLE II. Fitted values of parameters for extraction of fold-gated multiplicity distribution.

E_{beam} (MeV)	M_0	δM	J_0 ($\hbar$)
125	17	3.0	38
140	25	3.1	54

chance coincidence effects. The spectra were finally binned in energy bins of 1 MeV.

The experimental γ-ray fold distributions at beam energies of 125 and 140 MeV are shown in Fig. 2. Conversion of the fold distribution to angular momentum distribution was performed in two steps. The first step involved conversion of fold distributions to multiplicity distributions. The simulated fold distributions for different beam energy data were generated using the equation

$$P(F) = \sum_{M=0}^{M_{\max}} S(F, M) P(M). \tag{1}$$

The response matrix of the spin spectrometer, used for folding the multiplicity distribution, was obtained using the recursive algorithm given in Ref. [7]. This formalism takes care of the efficiency and crosstalk probability of the array. The form of multiplicity distribution *P(M)* used for input was given by

$$P(M) = \frac{2M + 1}{1 + \exp\left(\frac{M - M_0}{\delta M}\right)} \tag{2}$$

with M_0 and δM being two free parameters. The variables M_0 and δM were varied till resulting spectra matched with the experimental fold spectra. The fitted values of parameters for different beam energies are shown in Table II.

A low-multiplicity component with $M_0 = 6.0$ and $\delta M = 0.9$ has been added to match the high experimental yield in the lower-fold region. This contribution may be due to nonfusion events in the reaction. The effect of this contribution is negligible at higher folds. To avoid any contamination from these events, folds greater than 7 were considered for extracting high-energy γ-ray spectra for 140 MeV and folds greater than 9 for 125 MeV beam energy. The simulated folds, generated by this procedure, were compared with experimental fold

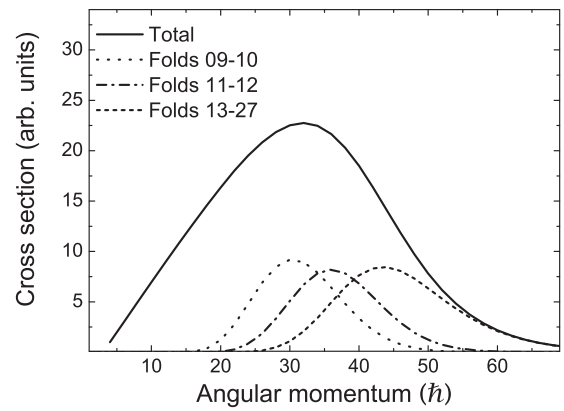

FIG. 3. Angular momentum distributions corresponding to different fold bins at 125 MeV beam energy.

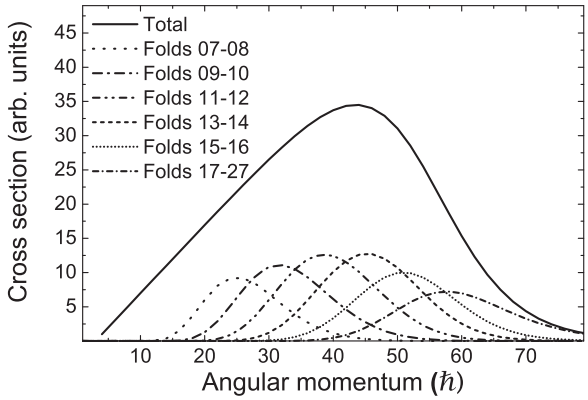

FIG. 4. Angular momentum distributions corresponding to different fold bins at 140 MeV beam energy.

distributions in Fig. 2. The second step involved the conversion of the multiplicity distribution to an angular momentum distribution using the relation [4] $J = 2M + k$, where k takes into account the angular momentum removed by statistical γ rays, particle emission, and γ rays below the trigger threshold. In present calculations $k = 4$ is used. The error induced in angular momentum calculation by this procedure remains within the experimental uncertainty. The angular momentum distributions were thus generated for different fold bins as $P(M) = S(F, M)P(F)$ and are shown in Fig. 3 for 125 MeV data and in Fig. 4 for 140 MeV data. These distributions were used as input [5] in the CASCADE calculations for extracting fold-gated GDR parameters as discussed in the next section.

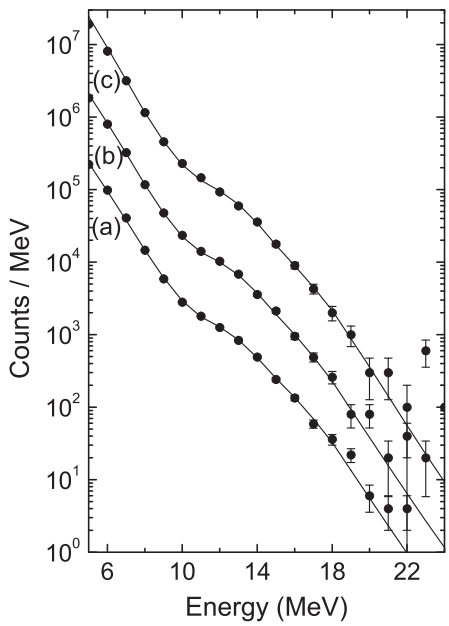

FIG. 5. High-energy γ-ray spectra gated with different fold bins at 125 MeV beam energy. Plots correspond to (a) folds 9–10, (b) folds 10–11, and (c) folds 13 and above. Each γ-ray spectrum was multiplied by 10 compared with the previous for representation on a single graph. Solid lines are the CASCADE calculations incorporating the GDR parameters folded with detector response.

B. Statistical model analysis

The experimental high-energy γ-ray spectra corresponding to different fold bins, viz., folds 9-10, 11-12, and 13 and above for 125 MeV energy, and folds 7-8, 9-10, 11-12, 13-14, 15-16, and 17 and above for 140 MeV energy data, are shown in Figs. 5 and 6, respectively. These fold-gated spectra were fitted with a statistical model using a modified version of the statistical model code CASCADE [20]. The relevant parameters used in CASCADE calculations are discussed below. The J distributions generated by gating different fold bins were used as the input angular momentum distribution in the code. The partial cross section for each fold bin was calculated by using the ratio of the area of each J distribution to the total area under the J distribution as shown in Figs. 3 and 4 and multiplied by the fusion cross section (Table I) for the reaction. This value was used by the code to normalize the input J distribution. The Reisdorf level density prescription [26] was used for all the calculations. The asymptotic level density parameter used was $\tilde{a} = A/8.5$ MeV^{-1} which is consistent with the values of 8.0 to 9.5 used in this mass range [5,6]. The angular momentum dependence of moment of inertia $\mathcal{I}$ in CASCADE is taken as $\mathcal{I} = \mathcal{I}_0(1 + \delta_1 J^2 + \delta_2 J^4)$.

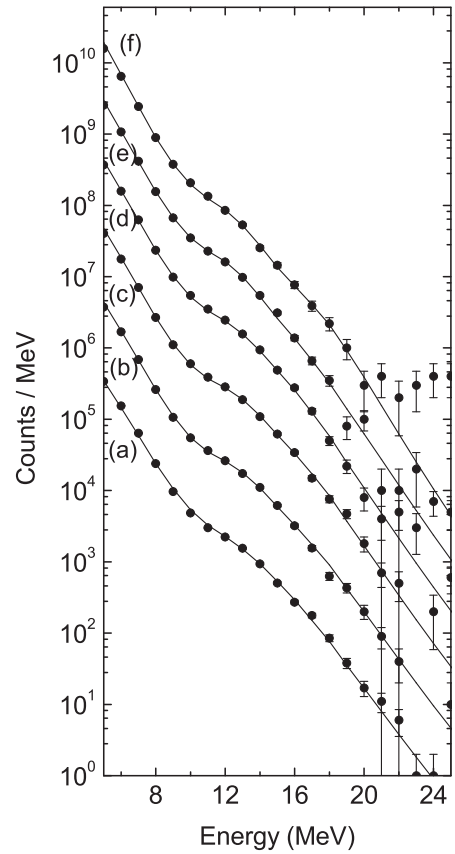

FIG. 6. High energy γ-ray spectra gated with different fold bins at 140 MeV beam energy. Plots corresponds to (a) folds 7–8, (b) folds 9–10, (c) folds 11–12, (d) folds 13–14, (e) folds 15–16, and (f) folds 17 and above. Each γ-ray spectrum was multiplied by 10 compared with the previous for representation on a single graph. Solid lines are the CASCADE calculations incorporating the GDR parameters folded with detector response.

TABLE III. Average angular momenta (J_{ave}) values for different fold bins and their corresponding standard deviations (σ_J).

E_{beam} (MeV)	Fold	J_{ave} ($\hbar$)	σ_J ($\hbar$)
125	9–10	30.7	6.17
125	11–12	36.2	6.57
125	13–27	45.0	9.41
140	7–8	25.9	6.21
140	9–10	32.4	6.99
140	11–12	38.9	7.47
140	13–14	45.1	7.73
140	15–16	50.9	8.00
140	17–27	59.2	9.79

The default values for this system were calculated to be $\delta_1 = 0.2137 \times 10^{-4}$ and $\delta_2 = 0$. The optical model potential parameters for the calculation of the transmission coefficients for the neutron, proton, and alpha particle have been taken from Refs. [27–29].

The GDR strength function was parametrized as a two-component Lorentzian [5,6] function with each component given by

$$F_L(E_\gamma, E_C, \Gamma) = \frac{\Gamma^2 E_\gamma^2}{\left(E_\gamma^2 - E_C^2\right) + \Gamma^2 E_\gamma^2}. \quad (3)$$

The effective transmission coefficient for γ-ray decay competing with particle decay in a statistical evaporation can be written as

$$T(E_\gamma) = C\frac{NZ}{A}E_\gamma^2 \frac{S_1 F_L(E_\gamma, E_1, \Gamma_1)}{\Gamma_1} + C\frac{NZ}{A}E_\gamma^2 \frac{S_2 F_L(E_\gamma, E_2, \Gamma_2)}{\Gamma_2} \quad (4)$$

with $C = 20.9 \times 10^{-6}$ MeV^{-1}. $E_{1(2)}$, $\Gamma_{1(2)}$, and $S_{1(2)}$ are resonance centroid energy, width, and strength of the respective Lorentzian function. Total strength is assumed to exhaust 100% of the sum-rule strength, i.e., $S_1 + S_2 = 1$. The CASCADE output, after varying six parameters $E_{1(2)}$, $\Gamma_{1(2)}$, and $S_{1(2)}$, was folded with detector response and compared with the experimental data. The goodness of fit was assured by minimizing χ^2 in the energy range of 9–20 MeV. The fit parameters obtained by this procedure are tabulated in Table IV. The errors in these parameters were obtained by varying the parameters to get the best fit within error limits of experimental data. For a better comparison of data, linearized plots [5] were obtained as $(Y_{exp}/Y_{cal}) \times F_{2L}$, where Y_{exp} is the experimental high-energy γ-ray yield, Y_{cal} is the CASCADE output folded with detector response, and F_{2L} is the two-component Lorentzian strength function. The high-energy γ-ray plots for different fold gates, fitted with CASCADE calculations, are shown in Figs. 5 and 6.

C. Temperature estimation

Since in the experiments the GDR decay at high excitation energy is observed as an average over several nuclear excited states, only the dependence of GDR parameters on the average temperature and angular momenta can be studied. To study the effect of temperature on GDR quantitatively, the GDR parameters are defined as a function of average angular momentum (J_{ave}) and average temperature (T_{ave}) of the excited nuclei. The J_{ave} is considered to be the average of the J distribution used for different folds. The T_{ave} [5] of the excited nuclear state on which GDR was built has been estimated using CASCADE for each fold-gated spectra. The partial temperature T_i of each nucleus in the decay chain was calculated using CASCADE as

$$T_i = \sqrt{\frac{E_i^* - E_i^{rot} - E_D - \Delta}{\tilde{a}}} \quad (5)$$

where E_i^* is Excitation energy of ith decay step, E^{rot} is the rotational energy of the system, computed at the average angular momentum of the each analyzed fold, E_D is GDR centroid energy for the respective fold, $\tilde{a} = A/8.5$ is the asymptotic level density parameter, and Δ is the pairing energy. The average temperature of the decay cascade is defined as $T_{ave} = \Sigma w_i T_i / \Sigma w_i$, where w_i is the weight for the ith step in the decay chain and was calculated as the γ-ray yield in the energy range of 12–20 MeV, dominated by GDR. The error in angular momentum calculations will, thus, be reflected in the estimated temperature values.

IV. RESULTS AND DISCUSSION

The experimental data was evaluated for different combinations of a two-component Lorentzian function by varying the

TABLE IV. GDR parameters extracted for different fold bins at two beam energies using the statistical model code CASCADE. Total strength is fixed at 100%, i.e. $S_1 + S_2 = 1$.

E_{beam} (MeV)	Fold	E_1 (MeV)	Γ_1 (MeV)	E_2 (MeV)	Γ_2 (MeV)	Strength S_2
125	9–10	12.8± 0.1	3.8 ± 0.1	16.3 ± 0.4	6.5 ± 0.4	0.66 ± 0.03
125	11–12	12.8± 0.2	3.6 ± 0.1	16.3 ± 0.3	5.8 ± 0.4	0.65 ± 0.02
125	13–27	13.0± 0.1	4.2 ± 0.2	16.5 ± 0.4	6.2 ± 0.2	0.62 ± 0.03
140	7–8	12.9± 0.1	4.9 ± 0.2	16.3 ± 0.2	7.4 ± 0.4	0.66 ± 0.04
140	9–10	13.1± 0.1	4.2 ± 0.2	16.5 ± 0.2	7.4 ± 0.4	0.66 ± 0.03
140	11–12	12.7± 0.2	3.8 ± 0.1	16.4 ± 0.3	6.5 ± 0.5	0.67 ± 0.02
140	13–14	12.7± 0.1	3.8 ± 0.2	16.2 ± 0.2	6.5 ± 0.5	0.65 ± 0.02
140	15–16	12.5± 0.1	3.6 ± 0.1	16.3 ± 0.3	7.8 ± 0.4	0.69 ± 0.02
140	17–27	12.7± 0.1	4.4 ± 0.1	17.5 ± 0.5	6.2 ± 0.2	0.62 ± 0.03

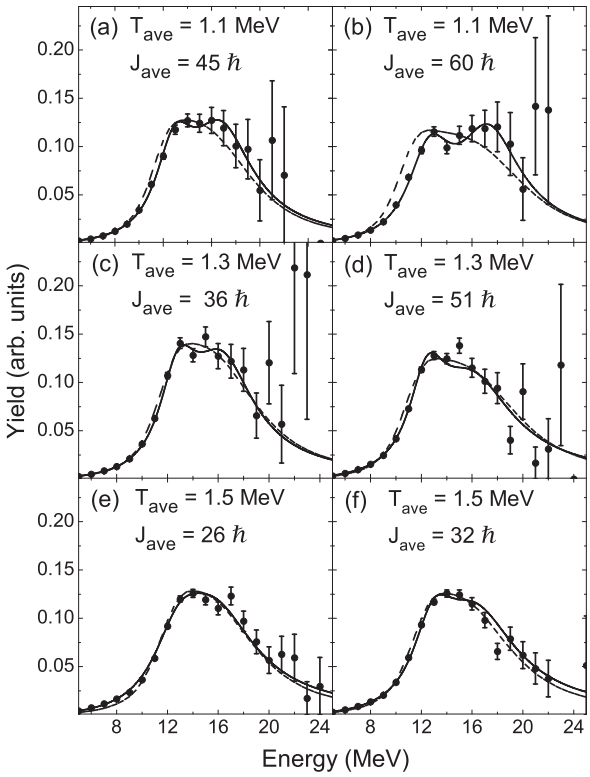

FIG. 7. Fold-gated linearized plots corresponding to different T_{ave} and J_{ave} combinations. The fold-to-J_{ave} correlation is tabulated in Table III. Solid lines represent the CASCADE calculations incorporating six-parameter GDR strength functions. Linearized plots were generated as $(Y_{exp}/Y_{cal}) \times F_{2L}$. Dashed lines are TSFM calculations. See text for details.

ratio of strengths S_1 and S_2. On the basis of χ^2 minimization, the best fit was obtained for the ratio $\frac{S_1}{S_2}$ close to 0.5. The extracted parameters for GDR are tabulated in Table IV. From the fitted parameters of GDR used in CASCADE and the linearized plots (shown in Fig. 7), GDR centroid energy E_D, width Γ_D, and deformation parameter β were extracted. The GDR centroid energy E_D is defined as the weighted average of two resonance centroids and is given by the expression $E_D = (S_1E_1 + S_2E_2)/(S_1 + S_2)$. The width is defined as the full width at half maximum (FWHM) of the two-component GDR strength function. The effective quadrupole deformation parameter β was calculated by the expression given in Refs. [3,30],

$$\beta = \sqrt{\frac{4\pi}{5}}\left(\frac{E_2/E_1 - 1.0}{0.5E_2/E1 + 0.87}\right). \quad (6)$$

The extracted GDR centroid, width, and deformation parameter are shown in Fig. 8 as a function of fold. The energy centroid was found to be nearly constant at 15.2 ± 0.3, whereas width and deformation changes with folds greater than 15. The effects of J_{ave} and T_{ave} on GDR observables are also tabulated in Table V. In next paragraph, we will compare the experimental results with theoretical calculations as a function of angular momentum.

TABLE V. Extracted GDR centroid energy E_D, width Γ_D, and deformation β for different average angular momentum and temperature values.

J_{ave} ($\hbar$)	T_{ave} (MeV)	E_D (MeV)	Γ_D (MeV)	β
30.7	1.33	15.1 ± 0.3	8.2 ± 0.5	0.28 ± 0.03
36.2	1.27	15.1 ± 0.2	8.2 ± 0.4	0.29 ± 0.02
45.0	1.14	15.2 ± 0.2	8.4 ± 0.5	0.28 ± 0.03
25.9	1.53	15.1 ± 0.3	8.8 ± 0.5	0.27 ± 0.03
32.4	1.47	15.2 ± 0.2	8.7 ± 0.5	0.28 ± 0.02
38.9	1.41	15.1 ± 0.2	8.5 ± 0.4	0.31 ± 0.03
45.1	1.33	15.0 ± 0.3	8.3 ± 0.4	0.29 ± 0.02
50.9	1.30	15.2 ± 0.2	9.0 ± 0.5	0.32 ± 0.03
59.2	1.14	15.5 ± 0.4	9.8 ± 0.6	0.38 ± 0.04

When the nucleus is in an excited state, the effective GDR cross sections and lineshapes carry information of the relative time scales for shape rearrangements that lead to shape fluctuations. We have performed TSFM calculations incorporating these fluctuations [15–17], where the averaged value of GDR cross section (σ) is calculated as

$$\langle\sigma\rangle_{\beta,\gamma} = \frac{\int \mathcal{D}[\alpha] \exp\{-F(T, J; \beta, \gamma)/T\} \Im_{TOT}\, \sigma(\beta, \gamma)}{\int \mathcal{D}[\alpha] \exp\{-F(T, J; \beta, \gamma)/T\} \Im_{TOT}} \quad (7)$$

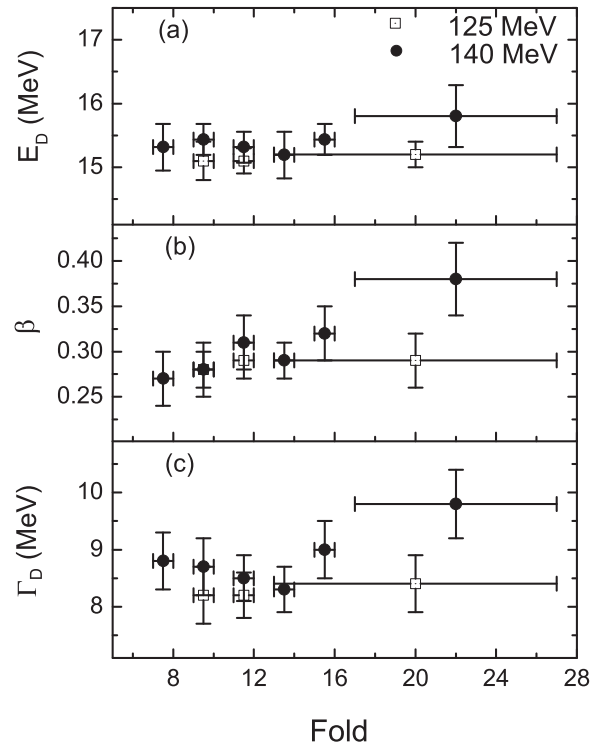

FIG. 8. Plots showing (a) GDR centroid energy E_D, (b) deformation parameter β, and (c) GDR width Γ_D as a function of fold for different beam energies. The error bars shown in the x-axis direction are the ranges of folds spanned for each data point.

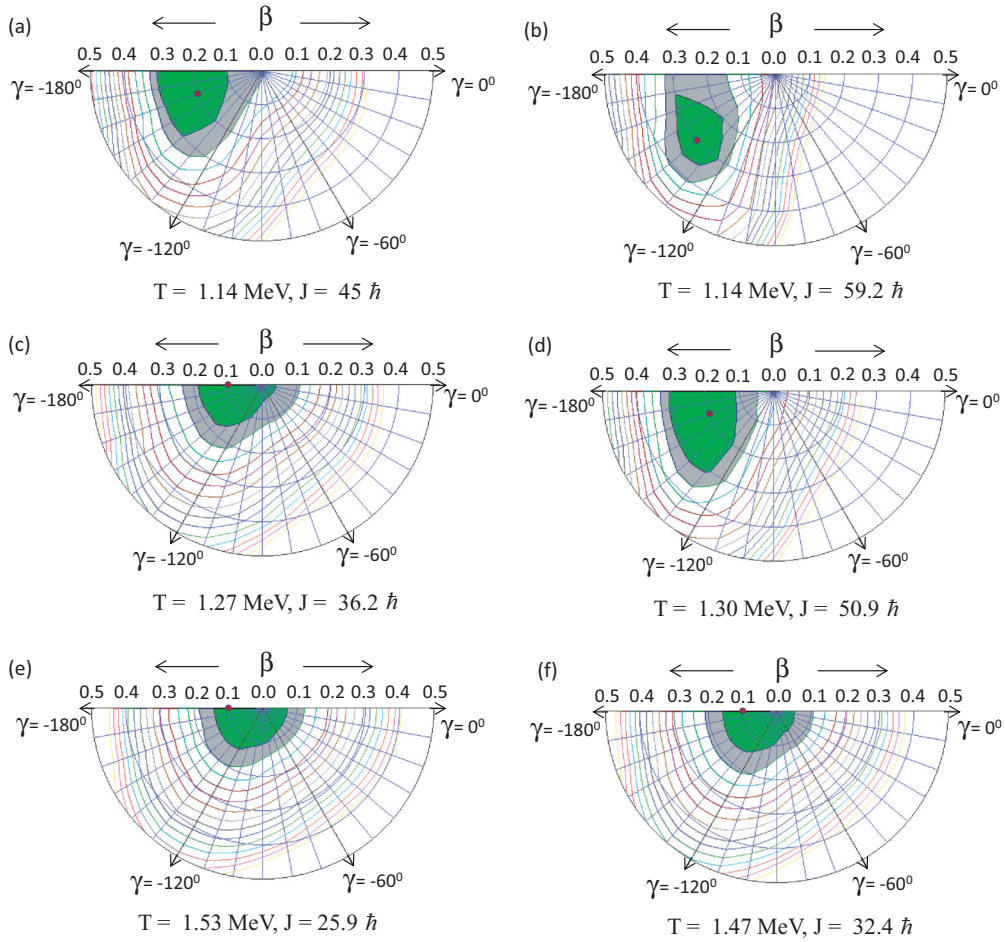

FIG. 9. (Color online) Potential energy surfaces of the nucleus ^{144}Sm at different angular momentum (J) and temperature (T). The contour line spacing is 0.5 MeV. The equilibrium shape is represented by a filled circle and the first two minima are shaded. The T and J values used in calculations are mentioned for each plot. The γ softness in the nuclei is visible from these plots.

with $\mathcal{D}[\alpha] = \beta^4 |\sin 3\gamma| \, d\beta \, d\gamma$, and $\Im_{\rm TOT}$ represents the moment of inertia inclusive of shell and surface diffuseness corrections. The GDR cross sections calculated by this method are plotted with experimental results in Fig. 7 and are denoted with a dotted line.

The free energy (F) is calculated by the finite-temperature cranked Nilsson-Strutinsky method (FTCNSM) where the dependence of shell corrections on temperature (T) and angular momentum (J) are taken care properly in a numerically exact method [15]. The GDR cross section at a fixed deformation (β, γ) is calculated in a macroscopic way [31] comprising an anisotropic harmonic oscillator potential with separable dipole-dipole interaction. In this formalism the GDR Hamiltonian could be written as

$$H = H_{\rm osc} + \eta \, D^{\dagger} D \tag{8}$$

with the parameter η characterizing the isovector component of the neutron and proton average field. The value of parameter η is varied such that the ground state GDR centroid energy is reproduced. In the case of ^{144}Sm, η was fixed at 3.0. The calculated cross sections, by this formalism, match the experimental data as can be seen in Fig. 7. Theoretical GDR widths were extracted from the FWHM of these cross section plots. The potential energy surfaces (PES) calculated for ^{144}Sm at the same experimental $J_{\rm ave}$ and $T_{\rm ave}$ values are plotted in Fig. 9. It can be seen from these plots that there is a shift in deformation at different $J_{\rm ave}$ values, and this isotope exhibits shape coexistance in the temperature range of 1.1–1.5 MeV. The values of average β were calculated as the ensemble weighted average over all possible deformations.

To disentangle the effect of angular momentum and temperature in the reaction, we have plotted experimental data points for different $T_{\rm ave}$ bins as a function of $J_{\rm ave}$. The temperature bins were taken for similar values of $T_{\rm ave}$ as given in Table V. The effect of angular momentum on GDR parameters at $T_{\rm ave}$ of 1.1, 1.3, and 1.5 MeV is shown in Fig. 10. The solid lines represents the TSFM calculations using the method described before. The experimentally observed centroid energy for different $J_{\rm ave}$ remained nearly constant. In the three $T_{\rm ave}$ bins, we further subdivide our findings in different J ranges. For 1.1, 1.3, and 1.5 MeV temperature, the corresponding angular momenta range were 45–59 $\hbar$, 30–50 $\hbar$, and 25–40 $\hbar$, respectively. As can be seen in Fig. 7, there

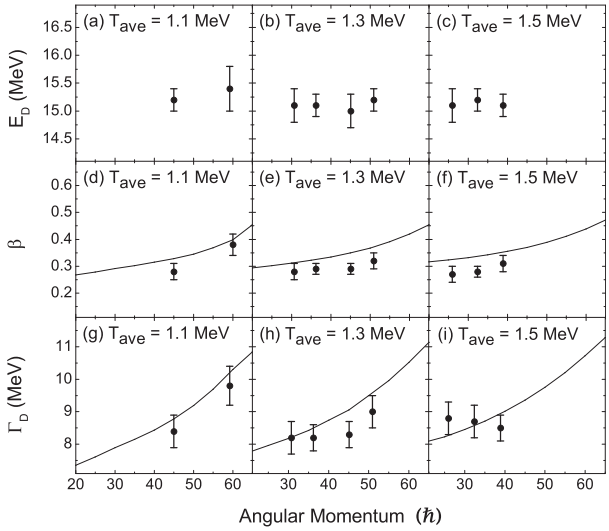

FIG. 10. GDR centroid energy (E_D), deformation parameter (β), and width (Γ_D) as a function of average angular momentum (J_{ave}) at different temperature (T_{ave}) bins. Circles denote experimental data. Solid lines in β curves are the ensemble-weighted averages of all possible calculated deformations. Solid lines in GDR width plots were extracted as FWHM of calculated cross sections based on TSFM.

is distinct splitting in experimental GDR strength functions at high J values in $T = 1.1$ MeV data. The minima in free energy calculations (represented as dot in PES curves) also shift towards high deformation in PES plots. In the case of 1.3–1.5 MeV, the values of Γ_D in the given experimental range remain nearly constant but not substantially different from TSFM calculations. Only at 1.1 MeV is there a trend of Γ_D increasing at high spin values. As in Fig. 10, the theoretically calculated β values from PES curves (depicted as solid lines) are 10% higher than the experimental points, although the trend of variation with J in both cases is the same. This slight deviation may be attributed to the method of averaging of β over different shapes in two cases.

The experimentally observed GDR widths at finite T and J [$\Gamma(T, J)$] have also been deduced by several authors [4,6] in terms of reduced width (Γ_{red}) given by Kusnezov *et al.* [18], who defined the reduced GDR width as

$$\Gamma_{red} = \left[\frac{\Gamma(T,J)}{\Gamma(T,0)}\right]^{\frac{T+3T_0}{4T_0}} \quad (9)$$

with

$$\Gamma(T,0) = \left(6.45 - \frac{A}{100}\right) ln\left(1 + \frac{T}{T_0}\right) + \Gamma_0(A), \quad (10)$$

where Γ_0(A) is the width for the spherical shape of the nucleus and T_0 was found to be 1 MeV. For describing the universal dependence of Γ_{red}, a universal parameter, reduced angular momentum ξ, was defined as $\xi = J/A^{5/6}$,

$$\Gamma_{red} = 1 + \frac{1.8}{1 + \exp\left(\frac{1.3-\xi}{0.2}\right)} \quad (11)$$

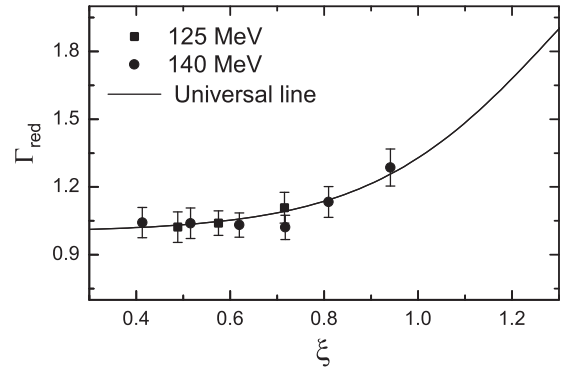

FIG. 11. GDR reduced width Γ_{red} as a function of reduced angular momentum ξ (J/A$^{5/6}$).

In the calculations, Γ_0 was adjusted for agreement with universal dependence for $\xi < 0.5$. This value was taken to be 3.8 MeV. The reduced widths, calculated using this parametrization for two different beam energies, are consistent with universal dependence, as shown in Fig. 11.

V. SUMMARY

High energy γ-rays in the range of 5–25 MeV have been measured in coincidence with the multiplicity of low-energy γ-rays for the compound nucleus ^{144}Sm. A wide range of angular momenta, from 25$\hbar$ to 60$\hbar$, has been covered at three different temperature bins of 1.1, 1.3, and 1.5 MeV for this nucleus. TSFM calculations have been performed for this nucleus using a numerically exact method and the calculated potential energy surface indicates the γ softness in this nucleus. The theoretical results match the experimental data for the GDR parameters within errors. The experimental GDR centroid energy obtained in this study in the temperature range of 1.1–1.5 MeV is found to be 15.2 ± 0.3 MeV which is close to the ground state value of 15.3 ± 0.1 [19]. The GDR width remained nearly constant for low spin values and showed an increasing trend at high values of angular momentum in the experimental range covered in conformity with TSFM calculations. Similar behavior is observed for the deformation parameter also. Kusnezov's parametrization is found to hold good for this nucleus at two different excitation energies.

ACKNOWLEDGMENTS

We would like to thank the Pelletron group of the IUAC, especially Rajan Joshi, for providing beams of excellent quality throughout the experiment and S.R. Abhilash for helping in fabrication of self-supporting Sm targets. We are thankful to Dr. S. R. Banerjee and Dr. Deepak Pandit for fruitful discussions on CASCADE calculations. Financial support from the University Grants Commission (UGC), Government of India, to one of the authors (I.M.) as Senior Research Fellow (SRF) is gratefully acknowledged.

[1] K. A. Snover, Annu. Rev. Nucl. Part. Sci. **36**, 545 (1986).
[2] J. J. Gaardhøje, Annu. Rev. Nucl. Part. Sci. **42**, 483 (1992).
[3] S. K. Rathi, D. R. Chakrabarty, V. M. Datar, S. Kumar, E. T. Mirgule, A. Mitra, V. Nanal, and H. H. Oza, Phys. Rev. C **67**, 024603 (2003).
[4] S. Bhattacharya, S. Mukhopadhyay, D. Pandit, S. Pal, A. De, S. Bhattacharya, C. Bhattacharya, K. Banerjee, S. Kundu, T. K. Rana, A. Dey, G. Mukherjee, T. Ghosh, D. Gupta, and S. R. Banerjee, Phys. Rev. C **77**, 024318 (2008).
[5] M. Kmiecik, A. Maj, A. Bracco, F. Camera, M. Casanova, S. Leoni, B. Million, B. Herskind, R. Bark, and W. Ormand, Nucl. Phys. A **674**, 29 (2000).
[6] D. Chakrabarty, V. Nanal, V. Datar, S. Kumar, A. Mitra, E. Mirgule, and R. Pillay, Nucl. Phys. A **770**, 126 (2006); D. R. Chakrabarty, V. M. Datar, S. Kumar, E. T. Mirgule, A. Mitra, V. Nanal, R. G. Pillay, and P. C. Rout, J. Phys. G: Nucl. Part. Phys. **37**, 055105 (2010).
[7] A. Maj, J. Gaardhøje, A. Ataç, S. Mitarai, J. Nyberg, A. Virtanen, A. Bracco, F. Camera, B. Million, and M. Pignanelli, Nucl. Phys. A **571**, 185 (1994).
[8] M. Mattiuzzi, A. Bracco, F. Camera, W. Ormand, J. Gaardhøje, A. Maj, B. Million, M. Pignanelli, and T. Tveter, Nucl. Phys. A **612**, 262 (1997).
[9] P. Bortignon, R. Broglia, G. Bertsch, and J. Pacheco, Nucl. Phys. A **460**, 149 (1986).
[10] P. Donati, N. Giovanardi, P. Bortignon, and R. Broglia, Phys. Lett. B **383**, 15 (1996).
[11] N. D. Dang and A. Arima, Phys. Rev. Lett. **80**, 4145 (1998).
[12] N. Dinh Dang, M. Ciemala, M. Kmiecik, and A. Maj, Phys. Rev. C **87**, 054313 (2013).
[13] M. Gallardo, M. Diebel, T. Døssing, and R. Broglia, Nucl. Phys. A **443**, 415 (1985).
[14] Y. Alhassid and B. Bush, Nucl. Phys. A **509**, 461 (1990).
[15] P. Arumugam, G. Shanmugam, and S. K. Patra, Phys. Rev. C **69**, 054313 (2004).
[16] P. Arumugam, A. Ganga Deb, and S. K. Patra, Euro. Phys. J. A **25**, 199 (2005).
[17] P. Arumugam, A. Ganga Deb, and S. K. Patra, Euro. Phys. Lett. **70**, 313 (2005).
[18] D. Kusnezov, Y. Alhassid, and K. A. Snover, Phys. Rev. Lett. **81**, 542 (1998).
[19] P. Carlos, H. Beil, R. Bergère, A. Leprêtre, A. D. Miniac, and A. Veyssière, Nucl. Phys. A **225**, 171 (1974).
[20] F. Pühlhofer, Nucl. Phys. A **280**, 267 (1977).
[21] I. Mazumdar, P. Sugathan, J. Das, D. Kataria, N. Madhavan, and A. Sinha, Nucl. Instrum. Methods Phys. Res. A **417**, 297 (1998).
[22] Y. K. Agarwal, C. V. K. Baba, D. R. Chakrabarty, and V. M. Datar, Pramana J. Phys. **35**, 49 (1990).
[23] S. Agostinelli *et al.*, Nucl. Instrum. Methods Phys. Res. A **506**, 250 (2003).
[24] G. A. Kumar, I. Mazumdar, and D. A. Gothe, Nucl. Instrum. Methods Phys. Res. A **611**, 76 (2009).
[25] E. T. Subramaniam, B. P. A. Kumar, and R. K. Bhowmik (unpublished).
[26] W. Reisdorf, Z. Phys. **300**, 227 (1981).
[27] D. Wilmore and P. Hodgson, Nucl. Phys. **55**, 673 (1964).
[28] F. G. Perey, Phys. Rev. **131**, 745 (1963).
[29] L. McFadden and G. Satchler, Nucl. Phys. **84**, 177 (1966).
[30] M. Danos, Nucl. Phys. **5**, 23 (1958).
[31] G. Shanmugam and M. Thiagasundaram, Phys. Rev. C **39**, 1623 (1989).